Supporting Information (SI) for

Photocatalytic Regeneration of a Nicotinamide Adenine Nucleotide (NADH) Mimic with Water-Soluble Iridium(III) Complexes

Mirjam R. Schreier,[a,b,+] Björn Pfund,[a,+] Debora M. Steffen,[a] Oliver S. Wenger [a,b,*]

[a] Department of Chemistry, University of Basel, St. Johanns-Ring 19, 4056 Basel, Switzerland

[b] National Competence Center in Research, Molecular Systems Engineering, 4002 Basel, Switzerland

[+] These two authors contributed equally to this work.

Corresponding author's e-mail address: oliver.wenger@unibas.ch

Contents

1. General Experimental Details

Materials

Unless otherwise indicated, the used chemicals were obtained commercially in high purity and were used as received. The investigated iridium(III) photosensitizers were available from some of our previous projects.[1, 2] The rhodium co-catalyst ([Cp*Rh(bpy)Cl]Cl)[3] and BNACl[4] were synthesized and characterized according to previously published procedures. 1,4-BNAH was synthesized by BNA^+ reduction using $Na_2S_2O_4$ and characterized according to a previous literature report.[5]

Ultrapure Millipore MilliQ water (specific resistance, 18.2 MΩ cm) was used for all spectroscopic measurements as well as for all photoinduced reductions. All solutions for optical spectroscopy and reductions were purged with argon (5.0, Pan Gas) for 5 minutes. To ensure stable pH conditions, a Tris-buffer (0.1 M, pH 8.8) or a phosphate-buffer (0.1 M, pH 7) was used.

Optical Spectroscopy

Steady-state UV-Vis absorption spectra were recorded with a Cary 5000 spectrometer (Varian). The Luminescence lifetime and quenching measurements were performed on a LifeSpec II spectrometer (Edinburgh Instruments) using the time-correlated single-photon counting (TCSPC) technique. The excitation source was a 405 nm picosecond pulsed diode laser (ca. 60 ps pulse width). Laser flash photolysis was performed on an LP920-KS apparatus from Edinburgh Instruments with 420 nm laser pulsed excitation (14 mJ per pulse) using a frequency-tripled Nd:YAG laser (Quantel Brilliant, ca. 10 ns pulse width) equipped with an OPO from Opotek. The kinetics at a single wavelength were recorded using a photomultiplier tube.

2. Photochemical Regeneration of 1,4-BNAH

The UV-Vis absorption spectra of the BNA^+ and 1,4-BNAH are shown in Figure S1A. Both BNA^+ (green trace) and 1,4-BNAH (orange trace) show absorption bands below 300 nm, but only 1,4-BNAH displays an absorption band in the range from 320 nm to 420 nm. By monitoring the absorption band maximum of 1,4-BNAH at 358 nm, the photochemical regeneration of BNAH from BNA^+ can be followed by UV-Vis absorption spectroscopy. To determine the effective concentration of the photochemically formed 1,4-BNAH, the extinction coefficient of that compound at 358 nm was first determined by measuring UV-Vis spectra at five different concentrations of 1,4-BNAH (Figure S1B). The absorbance at 358 nm was plotted against the concentration (Figure S1B, inset), resulting in a molar extinction coefficient at 358 nm (ε_{358}) of 5070 M^{-1} cm^{-1}. With the ε_{358} value at hand, the experimentally determined absorbance changes at 358 nm after given photo-irradiation times were determined. For this purpose, the initial absorbance value at 358 nm before irradiation was subtracted from the absorbance measured after a given irradiation time. This procedure is necessary, because the sensitizers and the rhodium(III) co-catalyst both have non-negligible extinction at that wavelength. The resulting optical density changes were then translated into concentrations of BNAH, using the Lambert-Beer law.

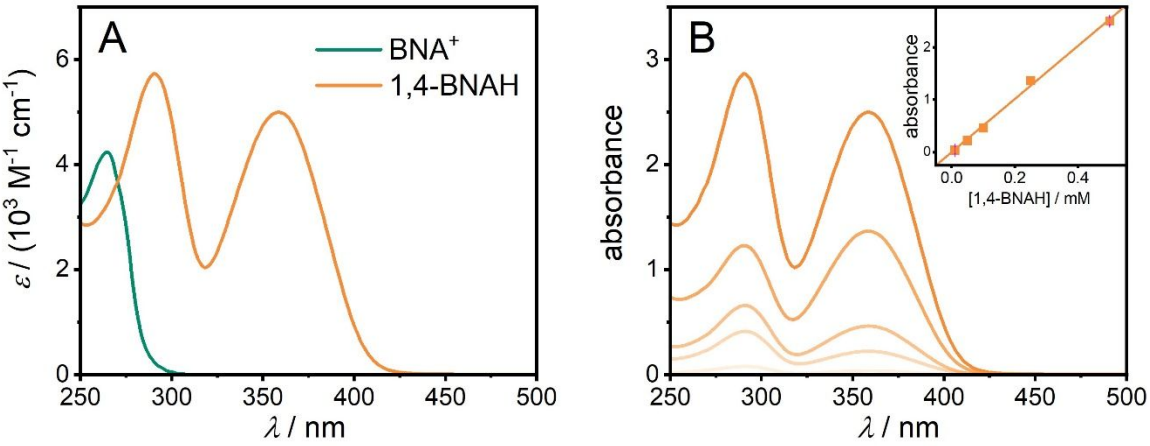

Figure S1. (A) Calibrated UV-Vis absorption spectra of BNA^+ (green trace) and 1,4-BNAH (orange trace) in deaerated phosphate buffer (0.1 M, pH 7) at 22 °C. These data sets are identical to those in Figure 2A of the main manuscript. (B) Determination of the molar extinction coefficient of 1,4-BNAH at 358 nm (ε_{358}). The main plot shows the UV-Vis absorption spectra at different concentrations of 1,4-BNAH in deaerated phosphate buffer (0.1 M, pH 7) at 22 °C, whereas the inset plots the absorbance at 358 nm as a function of 1,4-BNAH concentration; ε_{358} (5070 M^{-1} cm^{-1}) was determined from a linear regression fit to the experimental data in this plot.

For the photochemical regeneration of BNAH, solutions containing BNA^+ (1 mM, 1 eq.), $[Cp^*Rh(bpy)Cl]^+$ (0.1 mM, 10 mol%), photosensitizer (10 µM, 1 mol%), and TEOA (0.5 M) in deaerated phosphate buffer (0.1 M, pH 7) were irradiated in Schlenk-cuvettes using a 455 nm collimated LED (1.1 W, Thorlabs). The UV-Vis absorption spectra of the reaction mixture were measured after different time intervals (Figure S5). The formation of BNAH was tracked following the characteristic absorption band of BNAH at 358 nm. Using the extinction coefficient at 358 nm (ε_{358} = 5070 M^{-1} cm^{-1}), the yields of the photochemical reactions were estimated (Table S1).

To confirm that the photochemical reduction of BNA^+ to BNAH indeed occurs in regioselective 1,4-fashion,[6] ^{1}H-NMR experiments were performed under similar conditions. The outcome for $[Ir(sppy)_3]^{3-}$ is presented in Figure S2/S3/S4. Upon irradiation of the reaction mixture containing BNA^+ (10 mM), $[Cp^*Rh(bpy)Cl]^+$ (1 mM), TEOA (1.0 M), and the investigated photosensitizers (0.1 mM) in a 1:1 mixture of deaerated aqueous phosphate buffer (0.1 M, pH 7) and CD_3CN with the abovementioned 455 nm LED, the characteristic ^{1}H resonances of BNA^+ decrease with increasing irradiation time (Figure S2/S3/S4, orange backgrounds), while new signals attributable to 1,4-BNAH (green backgrounds) emerge. With the $[Cp^*Rh(bpy)(H_2O)]^{2+}$ co-catalyst, all photosensitizers gave exclusively the desired 1,4-BNAH product in yields of 82% ($[Ir(sppy)_3]^{3-}$), 86% ($[Ir(Fsppy)_3]^{3-}$), and 83% ($[Ir(dFsppy)_3]^{3-}$) after 6 hours in these ^{1}H-NMR studies, as summarized in Table S1.

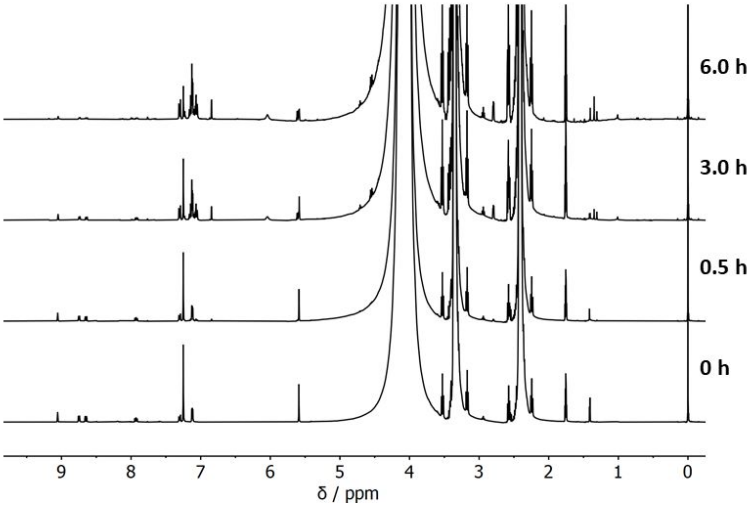

Figure S2. ^{1}H-NMR spectra monitoring the visible-light driven 1,4-BNAH regeneration from BNA^{+} (from the bottom to the top). The individual spectra were obtained after different irradiation times from a reaction mixture consisting of BNA^{+} (10 mM), $[Ir(sppy)_3]^{3-}$ (0.1 mM), $[Cp^*Rh(bpy)Cl]^{+}$ (1.0 mM), and TEOA (1.0 M) in a 1:1 mixture of non-deuterated deaerated aqueous phosphate buffer (0.1 M, pH 7) and CD_3CN. The irradiation source was a 455 nm LED. To monitor the growth of the product signals (1,4-BNAH) and the decrease of the proton resonances due to the starting material (BNA^{+}), spectral zooms between 1.4 and 3.5 ppm (Figure S3) as well as between 5.5 and 9.5 ppm (Figure S4) are further included.

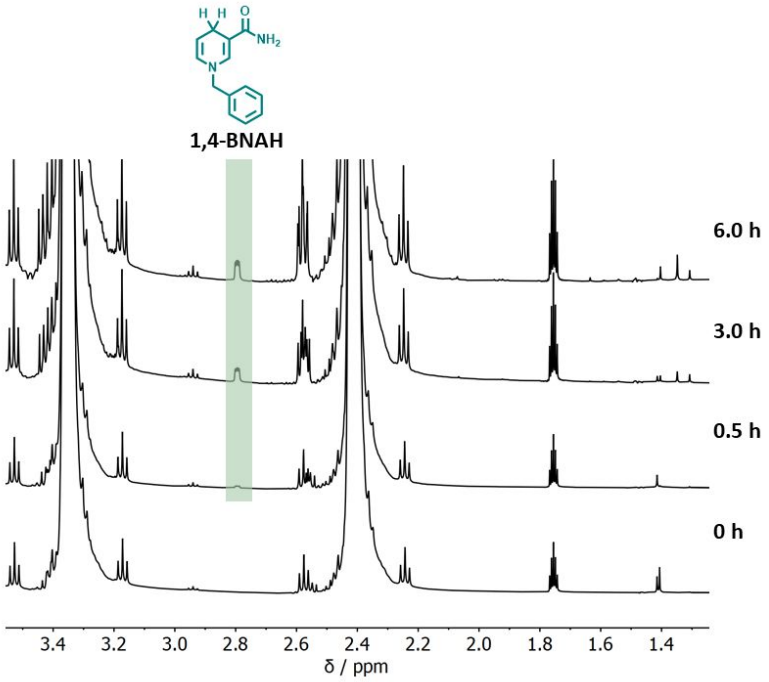

Figure S3. Zoom of the ^{1}H-NMR spectra monitoring the visible-light driven 1,4-BNAH regeneration from BNA^{+} (from the bottom to the top). The individual spectra were obtained after different irradiation times from a reaction mixture consisting of BNA^{+} (10 mM), $[Ir(sppy)_3]^{3-}$ (0.1 mM), $[Cp^{*}Rh(bpy)Cl]^{+}$ (1.0 mM), and TEOA (1.0 M) in a 1:1 mixture of non-deuterated deaerated aqueous phosphate buffer (0.1 M, pH 7) and CD_3CN. The irradiation source was a 455 nm LED. The characteristic signals of the cyclohexadienyl CH_2 group of 1,4-BNAH (green backgrounds) appear over time.

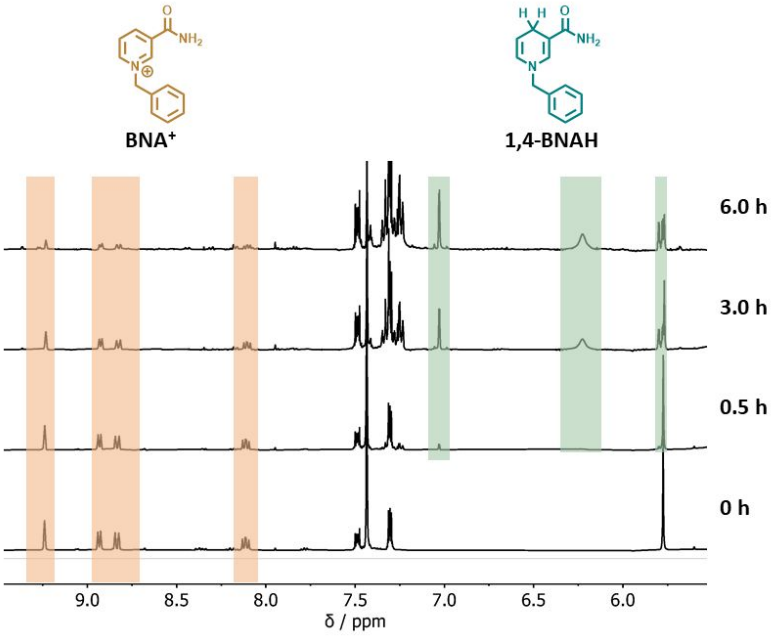

Figure S4. Zoom of the ^{1}H-NMR spectra monitoring the visible-light driven 1,4-BNAH regeneration from BNA^+ (from the bottom to the top). The individual spectra were obtained after different irradiation times from a reaction mixture consisting of BNA^+ (10 mM), $[Ir(sppy)_3]^{3-}$ (0.1 mM), $[Cp^*Rh(bpy)Cl]^+$ (1.0 mM), and TEOA (1.0 M) in a 1:1 mixture of non-deuterated deaerated aqueous phosphate buffer (0.1 M, pH 7) and CD_3CN. The irradiation source was a 455 nm LED. The characteristic signals of BNA^+ (orange backgrounds) decrease with increasing irradiation time, whereas the diagnostic resonances of 1,4-BNAH (green backgrounds) appear over time.

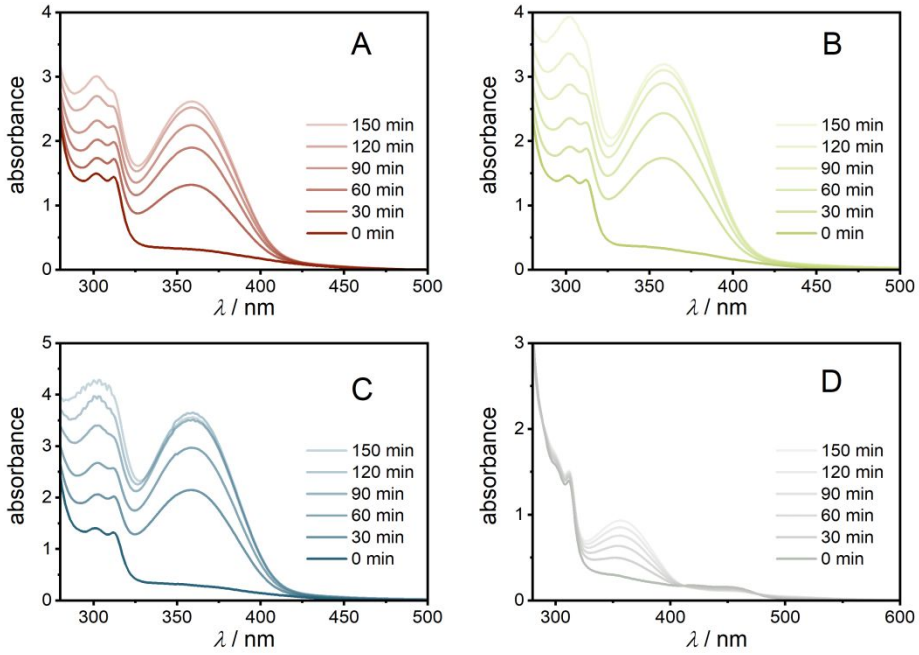

Figure S5. UV-Vis absorption spectra monitoring the visible-light driven BNAH regeneration from BNA^+ with different photosensitizers: $[Ir(sppy)_3]^{3-}$ (A), $[Ir(Fsppy)_3]^{3-}$ (B), $[Ir(dFsppy)_3]^{3-}$ (C), and $[Ru(bpy)_3]^{2+}$ (D). The different panels show the UV-Vis absorption spectra of reaction mixtures containing BNA^+ (1.0 mM), $[Cp^*Rh(bpy)Cl]^+$ (0.1 mM), TEOA (0.5 M), and the respective photosensitizers (10 µM) in deaerated aqueous phosphate buffer (0.1 M, pH 7) at 20 °C after different irradiation times, using the collimated output of a 455 nm LED as a light source.

Table S1. Summary of the photochemical formation of 1,4 BNAH with $[Cp^*Rh(bpy)Cl]^+$ and different sensitizers.

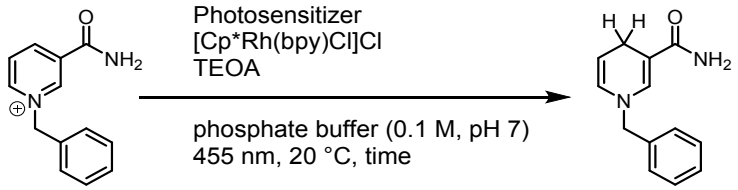

entry	photosensitizer	Yield of BNAH detected by UV-Vis spectroscopy [a, b] / %	Yield of 1,4-BNAH detected by ^{1}H-NMR spectroscopy [e, f] / %
1	$[Ir(sppy)_3]^{3-}$	46	82
2	$[Ir(sppy)_3]^{3-}$	0[d]	0
3	-	3.5[c]	0
4	$[Ir(Fsppy)_3]^{3-}$	56	86
5	$[Ir(dFsppy)_3]^{3-}$	64	83

[a] Reaction mixtures containing different photosensitizers (10 µM), BNA^+ (1.0 mM), $[Cp^*Rh(bpy)Cl]^+$ (0.1 mM) and TEOA (0.5 M) in deaerated aqueous phosphate buffer (0.1 M, pH 7) at 20 °C.

[b] The yield of 1,4-BNAH formation was determined based on the characteristic UV-Vis absorption band arising at 358 nm (ε_{358} = 5070 M^{-1} cm^{-1}) after 150 minutes of irradiation.

[c] The yield of 1,4-BNAH was determined after 160 minutes.

[d] Reaction mixture was kept in the dark.

[e] Reaction mixtures containing different photosensitizers (0.1 mM), BNA^+ (10 mM), $[Cp^*Rh(bpy)Cl]^+$ (1.0 mM) and TEOA (1.0 M) in a 1:1 mixture of CD_3CN and non-deuterated phosphate buffer (0.1 M, pH 7) at 20 °C.

[f] The yield of 1,4-BNAH was determined after 360 minutes.

3. Turnover Numbers and Turnover Frequencies

In the definition relevant to the work of this study, the turnover number (TON) describes the number of substrate molecules a catalyst can convert before it becomes inactivated. With our UV-Vis method to detect the formation of BNAH, the TON was determined from the optical density changes (before and after irradiation) at 358 nm (A_{358}), the extinction coefficient of 1,4-BNAH at that wavelength (ε_{358}), the path length of the cuvette (d), and the concentration of the iridium(III) photosensitizer (c_{PS}) or co-catalyst (c_{Rh}). Since a double catalytic system is postulated, separate TON values can be calculated for the photosensitizer (Equation S1) and the $[Cp^*Rh(bpy)(H_2O)]^{2+}$ (Equation S2). The factor of 2 in equation S1 reflects the fact that the reduction of BNA^+ to BNAH is a two-electron process and consequently requires two photosensitizer turnovers. The results are summarized in Table 2.

$$\mathrm{TON(PS)} = \frac{2 \times c_{\mathrm{BNAH}}}{c_{\mathrm{PS}}} = \frac{2 \times A_{358}}{\varepsilon_{358} \times d \times c_{\mathrm{PS}}} \tag{S1}$$

$$\mathrm{TON(Rh)} = \frac{c_{\mathrm{BNAH}}}{c_{\mathrm{Rh}}} = \frac{A_{358}}{\varepsilon_{358} \times d \times c_{\mathrm{Rh}}} \tag{S2}$$

The initial turnover frequency was determined as the number of cycles that the photosensitizer (PS) and the co-catalyst (Rh) performed within the first 30 minutes of the experiment:

$$\mathrm{TOF(PS)} = \frac{2 \times c_{\mathrm{BNAH}}}{c_{\mathrm{PS}} \times t} = \frac{2 \times A_{358}}{\varepsilon_{357} \times d \times c_{\mathrm{PS}} \times t} \tag{S3}$$

$$\mathrm{TOF(Rh)} = \frac{c_{\mathrm{BNAH}}}{c_{\mathrm{Rh}} \times t} = \frac{A_{358}}{\varepsilon_{357} \times d \times c_{\mathrm{Rh}} \times t} \tag{S4}$$

Table S2. Yields, turnover numbers (TONs), and initial turnover frequencies (TOFs) for the different photosensitizers and the rhodium co-catalyst (Rh) in the photochemical reduction of BNA^+ to BNAH.[a]

Photosensitizer (PS)	Yield of BNAH[b] / %	TON[c] (PS)	TON[c] (Rh)	Initial TOF[d] (PS) / h^{-1}	Initial TOF[d] (Rh) / h^{-1}
$[Ir(sppy)_3]^{3-}$	46	92	5	80	4
$[Ir(Fsppy)_3]^{3-}$	56	113	6	111	6
$[Ir(dFsppy)_3]^{3-}$	64	128	6	146	7
$[Ru(bpy)_3]^{2+}$	13	26	1	16	1

[a] Reaction mixture containing BNA^+ (1.0 mM), photosensitizer (10 μM), $[Cp^*Rh(bpy)Cl]^+$ co-catalyst (0.1 mM), and TEOA (0.5 M) in deaerated aq. phosphate buffer (0.1 M, pH 7) was irradiated with the collimated output of a 455 nm LED for 150 min.

[b] The yield of BNAH was determined by UV-Vis spectroscopy based on the characteristic absorption band arising at 358 nm (ε_{358} = 5070 M^{-1} cm^{-1}).

[c] The different turnover numbers (TONs) were determined based on the yield of BNAH after an irradiation time of 150 min.

[d] The different initial turnover frequencies (TOFs) were determined based on the yield of BNAH after an irradiation time of 30 min.

4. Mechanistic Studies

Photoluminescence quenching experiments with TEOA were performed using photosensitizer concentrations of 50 µM in aqueous deaerated deaerated phosphate buffer (0.1 M, pH 7) at 20 °C, following pulsed excitation at 440 nm. Luminescence decays at 510 nm were recorded in the absence of TEOA and in the presence of 1 M TEOA (Figure S6). $[Ir(sppy)_3]^{3-}$ and $[Ir(Fsppy)_3]^{3-}$ showed no emission lifetime quenching in this concentration range. $[Ir(dFsppy)_3]^{3-}$ showed a very low quenching efficiency η of 6.3% at 1 M TEOA concentration, based on τ_0 = 2110 and τ = 1980 ns at 1 M TEOA (using the relationship $\eta = (\tau_0 - \tau) / \tau$ given in the main paper). This results in an estimated quenching efficiency of 2% at 0.5 M TEOA used under the conditions of the UV-Vis experiments (Figure 2). Surprisingly, $[Ru(bpy)_3]^{2+}$ showed an 11% increase in the emission lifetime in the presence of 1 M TEOA, which could be attributable to a change in overall solvent properties when adding this much TEOA. A previous study reported a very low rate constant $k < 2 \times 10^5$ M^{-1} s^{-1} for electron transfer from TEOA to $^*[Ru(bpy)_3]^{2+}$ in water. Reductive excited-state quenching of $^*[Ru(bpy)_3]^{2+}$ could play a non-negligible role compared to the oxidative quenching with the rhodium co-catalyst (k_q = 1.2 × 10^8 M^{-1} s^{-1}) when TEOA is present at 0.5 M concentration and $[Cp^*Rh(bpy)(H_2O)]^{2+}$ is present at 0.1 mM (UV-VIS experiments, Figure S5) concentration.[7, 8]

Due to the low reaction rate constants for photoinduced electron transfer between the used iridium(III) sensitizers and TEOA, the reductive excited-state quenching reaction pathway for the iridium(III) complexes (right part of Figure 3) was neglected even at TEOA concentrations of up to 1 M. To investigate the oxidative excited-state quenching reaction pathway (left part of Figure 3), emission quenching experiments were performed using 50 µM solutions of photosensitizers in the presence of different concentrations of $[Cp^*Rh(bpy)(H_2O)]^{2+}$ (Figure S7). The bimolecular excited-state quenching rate constants (k_q) were obtained from linear regression fits in the Stern-Volmer plots (insets of Figure S7) and are summarized in Table 2 of the main manuscript.

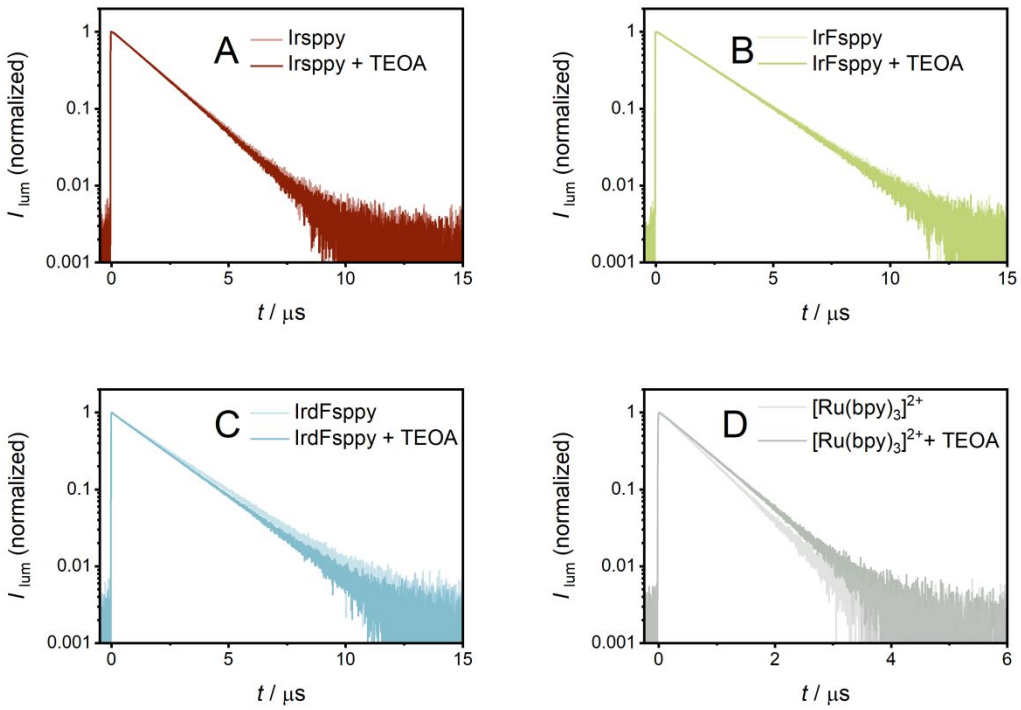

Figure S6: Luminescence decays of 50 µM $[Ir(sppy)_3]^{3-}$ (A), $[Ir(Fsppy)_3]^{3-}$ (B), $[Ir(dFsppy)_3]^{3-}$ (C), and $[Ru(bpy)_3]^{2+}$ (D) in neat solutions (light traces) and in the presence of 1 M TEOA (darker traces) in deaerated phosphate buffer (0.1 M, pH 7) at 20 °C after excitation at 440 nm with laser pulses (18 mJ). The emission decays were detected at the respective emission maxima at 510 nm (A), 500 nm (B), 490 nm (C), and (D) 610 nm.

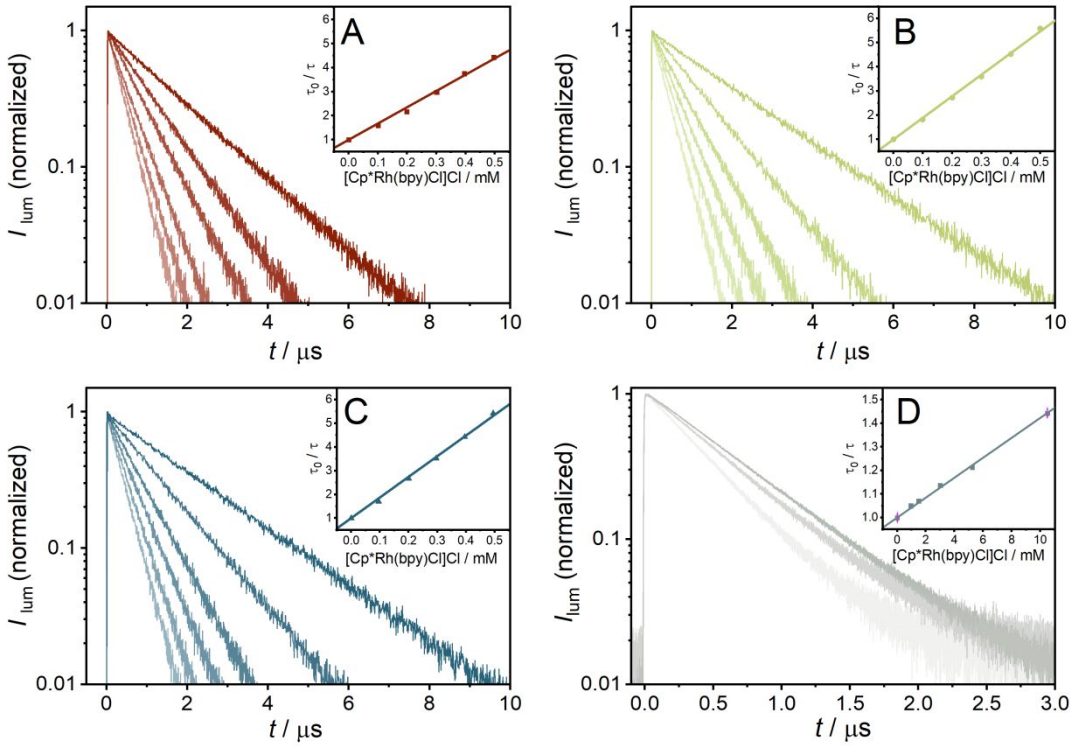

Figure S7. Time-resoled luminescence quenching experiments with 50 µM $[Ir(sppy)_3]^{3-}$ (A), $[Ir(Fsppy)_3]^{3-}$ (B), $[Ir(dFsppy)_3]^{3-}$ (C) and $[Ru(bpy)_3]^{2+}$ (D) at varying concentrations of $[Cp^*Rh(bpy)Cl]^+$. The main plots show the luminescence decays, whereas the insets represent the respective Stern-Volmer plots obtained from the data in the main plots. All quenching experiments were performed in deaerated aqueous Tris-buffer (0.1 M, pH 8.8) at 20 °C. The experiments displayed in panels A-C were performed using the TCSPC technique. Upon excitation at 405 nm, the kinetic emission decays were traced at the emission maxima at 510 nm (A), 500 nm (B), and 490 nm (C). The kinetic decay traces of (D) at 610 nm were measured by laser flash photolysis upon excitation at 420 nm, using laser pulse energies of 13 mJ.

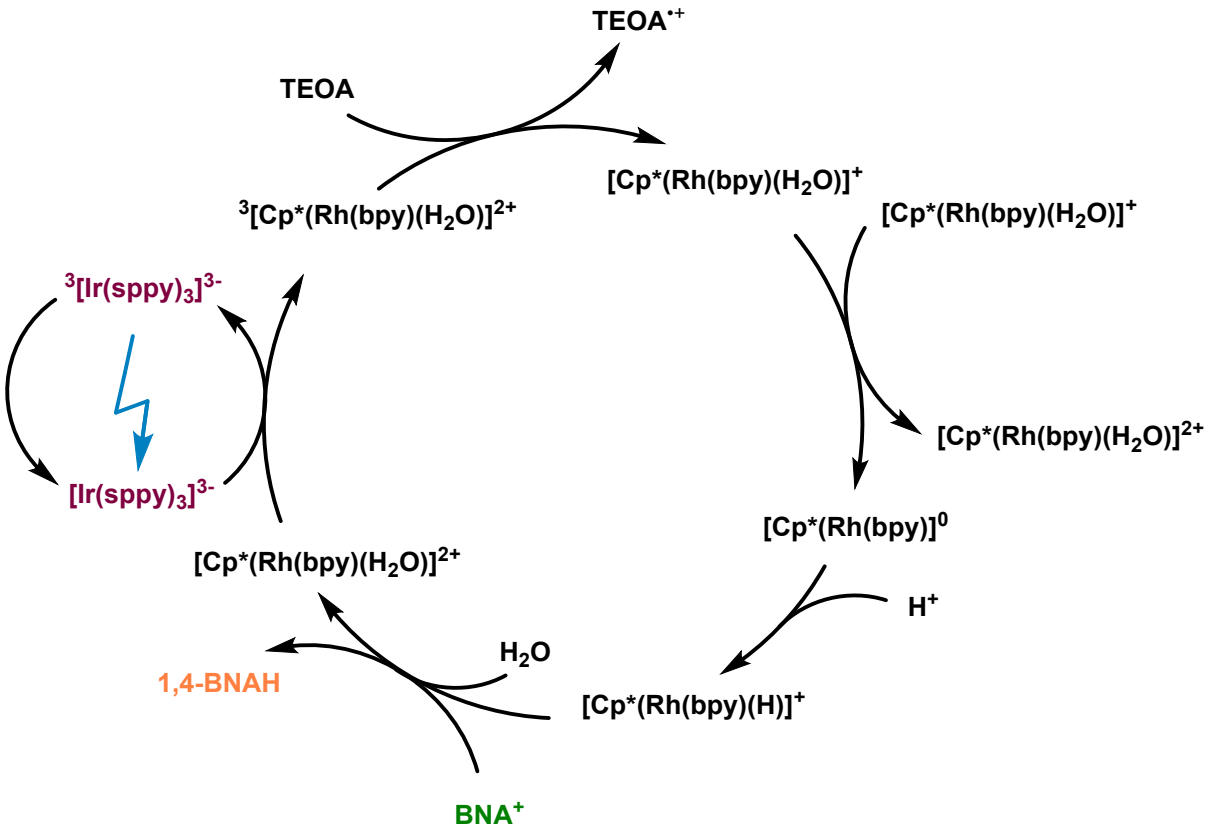

Figure S8. Considered triplet-triplet energy transfer (TTET) based reaction mechanism. Energy transfer from the excited iridium (III) sensitizer to $[Cp^*Rh(bpy)(H_2O)]^{2+}$, which is reductively quenched by TEOA to afford the Rh(II) form $[Cp^*Rh(bpy)(H_2O)]^{+}$. $[Cp^*Rh(bpy)(H_2O)]^{+}$ can disproportionate into Rh(III) and Rh(I) species. The latter, can be protonated to yield the key species $[Cp^*Rh(bpy)(H)]^{+}$, which performs the regioselective reduction of BNA^{+}, as reported previously.[9, 10] For simplicity, $[Ir(sppy)_3]^{3-}$ is depicted as a representative example for all three employed iridium(III) sensitizers.

5. References

1. Pfund, B.; Steffen, D. M.; Schreier, M. R.; Bertrams, M.-S.; Ye, C.; Börjesson, K.; Wenger, O. S.; Kerzig, C., UV Light Generation and Challenging Photoreactions Enabled by Upconversion in Water. *J. Am. Chem. Soc.* **2020,** *142*, 10468-10476, DOI: 10.1021/jacs.0c02835.

2. Guo, X.; Okamoto, Y.; Schreier, M. R.; Ward, T. R.; Wenger, O. S., Enantioselective synthesis of amines by combining photoredox and enzymatic catalysis in a cyclic reaction network. *Chem. Sci.* **2018,** *9*, 5052-5056, DOI: 10.1039/c8sc01561a.

3. Ghosh, T.; Slanina, T.; König, B., Visible light photocatalytic reduction of aldehydes by Rh(III)-H: a detailed mechanistic study. *Chem. Sci.* **2015,** *6*, 2027-2034, DOI: 10.1039/c4sc03709j.

4. Tan, H.; Wang, J.; Zhang, Y.; Xing, Y.; Sun, Q.; Li, R., Tandem synthesis of substituted 2,7-naphthyridin-1(7H)-ones via Reissert reaction/intramolecular nucleophilic addition/oxidation dehydrogenation. *Tetrahedron* **2013,** *69*, 8299-8304, DOI: 10.1016/j.tet.2013.05.105.

5. van Schie, M.; Paul, C. E.; Arends, I.; Hollmann, F., Photoenzymatic epoxidation of styrenes. *Chem. Commun.* **2019,** *55*, 1790-1792, DOI: 10.1039/c8cc08149b.

6. McSkimming, A.; Colbran, S. B., The coordination chemistry of organo-hydride donors: new prospects for efficient multi-electron reduction. *Chem. Soc. Rev.* **2013,** *42*, 5439-5488, DOI: 10.1039/c3cs35466k.

7. Rivarola, C. R.; Bertolotti, S. G.; Previtali, C. M., Photoreduction of $Ru(bpy)_3^{2+}$ by Amines in Aqueous Solution. Kinetics Characterization of a Long-Lived Nonemitting Excited Statet. *Photochem. Photobiol.* **2006,** *82*, 213-218, DOI: 10.1562/2005-05-31-RA-558.

8. Chan, S.-F.; Chou, M.; Creutz, C.; Matsubara, T. S., Norman Mechanism of the Formation of Dihydrogen from the Photoinduced Reactions of Poly(pyridine)ruthenium(II) and Poly(pyridine)rhodium(III) Complexes. *J. Am. Chem. Soc.* **1981,** *103*, 369-379, DOI: 10.1021/ja00392a022.

9. Lo, H. C.; Leiva, C.; Buriez, O.; Kerr, J. B.; Osmstead, M. M.; Fish, R. H., Bioorganometallic Chemistry. 13. Regioselective Reduction of NAD^+ Models, 1-Benzylnicotinamde Triflate and *β*-Nicotinamide Ribose-5'-methyl Phosphate, with in Situ Generated $[Cp^*Rh(Bpy)H]^+$: Structure-

Activity Relationships, Kinetics, and Mechanistic Aspects in the Formation of the 1,4-NADH Derivatives. *Inorg. Chem.* **2001,** *40*, 6705-6716, DOI: 10.1021/ic010562z.

10. Kölle, U.; Grützel, M., Organometallic Rhodium(III) Complexes as Catalysts for the Photoreduction of Protons to Hydrogen on Colloidal TiO_2. *Angew. Chem. Int. Ed* **1987,** *26*, 567-570, DOI: 10.1002/anie.198705671.